Dynamics of proton transfer reactions of model base pairs in the ground and excited states: Revisited

Fuke, Kiyokazu

Ishikawa, Haruki

(Citation)
Chemical Physics Letters,623:117-129

(Issue Date)
2015-03-02

(Resource Type)
journal article

(Version)
Accepted Manuscript

(URL)
https://hdl.handle.net/20.500.14094/90003495

Dynamics of Proton Transfer Reactions of Model Base Pairs in the Ground and Excited States: Revisited

Kiyokazu Fuke[a,b]*, Haruki Ishikawa[c]

[a] Department of Chemistry, Graduate School of Science, Kobe University, 1-1 Rokkodai, Nada-ku, Kobe 657-8501, Japan

[b]Institute for Molecular Science, 38 Nishigo-naka, Myodaiji, Okazaki 444-8585, Japan

[c]Department of Chemistry, School of Science, Kitasato University, 1-15-1 Kitasato, Minami-ku, Sagamihara 252-0373, Japan

Abstract

A review of the proton transfer reactions (PTR) of model base pairs such as the 7-azaindole and 1-azacarbazole dimers is presented, including some of the recent progress in the laser spectroscopy of these dimers. Advances in computational chemistry now allow to calculate reliable potential energy surfaces of the excited-state PTR, which is indispensable to understand the experimental results. The comprehensive results on the spectroscopy and reactivity of these dimers are outlined for fully explaining the excited state PTR of model base pairs on the basis of the current theoretical studies. Moreover, the recent studies on the PTR in the ground state relating to a back proton translocation of tautomeric dimer of 7-azaindole are presented. Finally, the outlook on the study of the PTR of model base pairs is addressed to further explore the reaction dynamics of these benchmark systems.

Corresponding author.

E-mail address: fuke@kobe-u.ac.jp (K. Fuke).

I. Introduction

Proton transfer reactions (PTR) have received much attention in recent years because of their widespread processes in molecular science [1-3]. Among them the excited-sate double proton transfer in the model base pairs such as 7-azaindole dimer $(7\text{-AI})_2$ is one of the most important benchmark systems studied in this context [4-6]. This dimer has also been claimed that it can be used as a prototype system to mimic the elementary reactions involved in the photomutagenesis in the DNA base pairs [1,6]. Because of its structural relation with 7-AI, 1-azacarbazole dimer, $(1\text{-AC})_2$, has also long been recognized as a model for the DNA base pairs and has attracted considerable interest as a model system to investigate the phototautomerism of 7-AI [7-9]. Figure 1 shows schematically the photo-tautomerization process of these dimers involving a double proton-transfer reaction, and the process has been thoroughly studied in solution with various laser spectroscopic techniques in order to understand whether this process can be of significance in mutagenesis [10-14]. However, in solution, the solvation effect blurred the spectroscopic details and the reaction features of model base pairs. To overcome these problems and to unveil the potential energy surfaces involved and the reaction dynamics progressed, the absorption and emission properties of $(7\text{-AI})_2$ and $(1\text{-AC})_2$ were examined in molecular beam since 1980's [15-18]. The dimers in supersonically cooled and isolated conditions allowed to get insight into the intrinsic nature of the excited-state PTR (ESPTR) such as the tunneling and vibrational mode specific reaction rates in addition to the information on the potential energy surfaces. Because the PTR rate of the excited-state $(7\text{-AI})_2$ is very fast, the spectral bandwidth are broaden, and therefore, the spectroscopic information to map out the potential energy surface is rather limited. On the other hand, $(1\text{-AC})_2$, whose PTR rate is much slower, provided us complimentary results on the spectroscopic and reaction properties of the excited-state dimer [17,18]. This dimer also allowed us to trace the PTR process with a picosecond time-resolved fluorescence technique and to confirm the implicitly assumed reaction mechanism such as the single step and/or concerted process [19].

In 1995, the mechanistic subject was refocused by Douhal, et al. [20]. They reported the time-resolved study of the ESPTR of $(7\text{-AI})_2$ in a molecular beam using a mass spectrometry coupled with a femtosecond laser pump-probe technique. Based on the observation of a bi-exponential decay at the dimer equivalent mass (236), they proposed a two-step process as an alternative reaction mechanism including an intermediate state; this new proposal for the mechanism is against the then-accepted scheme of the cooperative, single-step path. They also reexamined the ESPTR of $(7\text{-AI})_2$ in solution using a fluorescence gating technique and tried to interpret the observed two-component decay along with the similar scheme in the gas phase [21]. On the other hand, Tahara and Takeuchi, independently, examined the same system using a femtosecond fluorescence up-conversion technique and supported

the single-step mechanism [22]. Since then, for more than a decade, several experimental and theoretical groups, including Catalan' group [23], studied this reaction extensively and argued about the reaction mechanism. The details of these debates were reviewed in elsewhere [24]. The outline of these arguments is also presented in the later section together with the recent theoretical works on a reliable potential energy surface, which support the single-step mechanism [25,26].

Until now, most of the researches on the model base pairs were concerns with the excited-state PTR. However, $(7\text{-AI})_2$ is also considered to be a benchmark system for studying the PTR in the electronic ground states. In this system, the reaction product such as the tautomeric dimer was trapped in molecular beam [18,27,28] and also in solution [11,12,29,30]. In particular, a back PTR from the tautomer to the normal dimer was examined by the IR spectroscopy in molecular beam [27,28].

In the aforementioned debates, almost all of the studies were concerned with the mechanism of the PTR, but most of the important issues on the dynamical processes involved in these tautomerization reaction, which were pointed out in the earlier study [18], remained unsettled. In this article, we revisit the experimental results on the spectroscopy and the excited-state reaction process of model base pairs, and discuss the reaction energy surface and the dynamics of PTR, together with the current status of the computational results. We will also briefly summarize the recent results on the ground-state PTR which proceeds in the vibrationally excited state [27,28]. Finally, we may give an outlook on the study of the PTR processes of model base pairs to get further insight into the reaction dynamics of these systems.

The paper is organized as follows: In Section II we describe the PTR of model base pairs in the electronically excited state. We first summarize the spectroscopy of 7-AI; monomer and dimer in Section II-1-1, and 7-AI tautomeric dimer in Section II-1-2. In Section II-2 we describe the spectroscopy of 1-AC monomer and dimer. In Section II-3 we summarize the present status of the time resolved studies and mechanism of PTR in model base pairs. In Section II-4 we present the potential energy surface and dynamics of PTR in model base pairs; vibrational mode dependence of PTR in Section II-4-1, tunneling effect on PTR in Section II-4-2 and the outline of the recent theoretical studies on potential energy surface in Section II-4-3. In Section III we describe the PTR of $(7\text{-AI})_2$ in the electronic ground state. We first summarize the potential energy surface of the PTR of $(7\text{-AI})_2$ in Section III-1. Secondly, the IR spectroscopy of the 7-AI monomer and normal dimer in Section III-2. In Section III-3 we present the IR spectroscopy of the 7-AI tautomeric dimer and discuss the reactivity at the v = 1 level of the N—H stretching mode. In Section III-4 we describe the deuteration effects on the IR spectra of the normal and the tautomeric dimers. In Section IV we present the summary and the outlook of the studies on the PTR of model base pairs.

II. PTR of model base pairs in the electronically excited state

II-1. Spectroscopy of 7-AI

(II-1-1) Spectroscopy of 7- AI monomer and dimer

(7-AI monomer)

In order to understand the excited-state PTR, it is important to gain information on the electronic structures and the potential energy surfaces of the relevant excited states. To this end, the electronic spectra of the $S_1 - S_0$ transitions of 7-AI monomer and its dimer have been examined extensively in solution [4-6,10,13]. However, the spectrum is very broad and gives no detail information on the potential energy surface. This situation was changed in the 1980's with the advent of the supersonic molecular beam and laser spectroscopic techniques [16-18]. The spectrum of 7-AI monomer in molecular beam was examined by using the fluorescence excitation and dispersed fluorescence methods as well as the mass selected multi-photon ionization (MPI) technique. Figure 2a shows the fluorescence excitation spectrum of 7-AI monomer [16]. The vibronic progression started at 34639 cm^{-1} was assigned to the transition to the first $\pi\pi^*$ excited state from its spectral intensity. Since then, several research groups carried out high resolution spectroscopy for 7-AI monomer [31-34]. Hassan and Hollas [31] confirmed the assignment as the $\tilde{A}\ ^1A'$ ($\pi\pi^*$) — $X\ ^1A'$ transition. With a rotational band contour analysis, they determined the rotational constants for both electronic states and the transition dipole moment hybrid ratio. Schmitt and coworker also examined the rovibronic spectra of four isotopic species of 7-AI [33]. Using the inertial parameters, the structures of 7-AI in the S_0 and S_1 states have been determined; the expansion of the pyridine ring, not of the pyrrole ring, in the excited state was found. In order to understand the reactivity of the dimer, the electronic character of the lowest excited state of 7-AI monomer are important issues to be resolved, in particular on the mixing of the $n\pi^*$ state. These high resolution studies confirmed that the lowest transition is the L_b type and that the mixing of the $n\pi^*$ nature, which was suggested in earlier paper [35], is less important. Recently, an anomaly related to vibrational mixing was reported by Sakota and Sekiya, who showed that the N—H stretching frequency is significantly reduced when 7-AI is excited to the +280 cm^{-1} vibrational level of the S_1 state [36]. Pratt, et al. examined the permanent dipole moment of this vibronic band using the high resolution fluorescence spectroscopy coupled with a Stark-effect measurement [37]. They observed a large increase in the dipole moment, as large as by a factor 2 from that of the zero vibrational level, and they ascribed the increase to a mixing of the L_b state with a $\sigma\pi^*$-type state.

(7-AI dimer)

The earlier papers of the 7-AI dimer reported the spectroscopy for the S_1 - S_0 transition using the fluorescence excitation and MPI techniques [15,16]. The closely-lying two transitions, the origins of which were at 32252 and32290 cm^{-1}, were found; they had completely different spectral features [16]. The former transition exhibits broad vibronic bands, and, even at the origin excitation, a visible

fluorescence, peaking at 480 nm, was observed; the emission is similar to that of the tautomer observed in solution [4]. On the other hand, the sharp low-frequency vibronic bands follow the latter origin at 32290 cm^{-1}, and a fluorescence limited only to the UV region was observed by the excitation of these bands. In the later study, the transition having the origin at 32290 cm^{-1} was reassigned to a water complex of $(7\text{-AI})_2$ by measuring an IR spectrum, which exhibits a vibrational band characteristic to a non-hydrogen bonded O—H [38]. The water was considered to be readily dissociated in the ionic state to yield the $(7\text{-AI})_2$ dimer ion. Thus, in the following discussion, we only consider the dimer having the origin at 32252 cm^{-1}.

Figure 2b shows the fluorescence excitation spectrum of $(7\text{-AI})_2$ obtained by monitoring the visible fluorescence, which is the emission from the tautomer formed in the excited state through the PTR process; this figure is an action spectrum of the reaction product (tautomer) [18]. The origin at 32252 cm^{-1} is shifted by 2387 cm^{-1} from that of monomer. The large spectral shift was ascribed to the formation of two strong hydrogen bonds in the dimer. The theoretical calculations predicted that, upon the excitation, the pyrrolic N—H group becomes more acidic, while the basicity of the pyridino N atom increases [23]. These changes may lead to a considerable shortening of both hydrogen bonds between two 7-AI moieties in the excited state. In contrast to the monomer, it is difficult to get information on the electronic structure of the excited-state dimer from the high resolution spectroscopy, because the spectrum is broad even at the zero vibrational level. The band width of the 0 – 0 transition shown in Figure 2b was 5 cm^{-1}; it was revised as 2.7 cm^{-1} in the later study [39]. It is too broad to conduct the high resolution spectroscopy. In place of $(7\text{-AI})_2$, the rotationally-resolved electronic spectra of the electronic origins of 7-AI-water complexes were examined in molecular beam [32,40]. From the observed changes in the rotational constants upon electronic excitation and the orientation of the transition dipole, a solvent induced state reversal between the L_a and L_b states upon microsolvation was reduced [40]. Similarly to the 7-AI-water complexes, the second excited L_a state in 7-AI monomer is expected to be stabilized by the strong hydrogen bonds and becomes the lowest in $(7\text{-AI})_2$. From a simple exciton theory, the first excited state of monomer may split into two states (^{1}Bu and ^{1}Ag states in C_{2h} symmetry) upon dimer formation [18]. The ^1B_u state is optically allowed and the transition to this state corresponds to the observed spectrum in Figure2b. The nature of the lower-lying excited states of 7-AI dimer was also examined theoretically by several research groups [26]. Recently, Ando and his coworker also reported the theoretical results on the exciton coupling and the energies of these excited states [25]. According to their calculations, the energy difference between the two diabatic states is much larger than that of the off-diagonal coupling elements, and thus, $(7\text{-AI})_2$ is in the weak coupling regime. They predicted the difference in the vertical excitation energies of two excited states to be 0.02 eV. These predictions are consistent with the spectroscopic results on

monodeuterated $(7\text{-AI})_2$ [41].

As seen in Figure 2b, the electronic spectrum of $(7\text{-AI})_2$ in the energy region below 500 cm^{-1} from the band origin is rather simple [18]. Most of the vibronic bands are explainable by the fundamental, overtones, and combination bands of the intermolecular vibrational bands. Interestingly, the band widths of these vibronic bands rapidly change both with the vibrational modes and with the excitation energy. These observations clearly indicate that the intermolecular vibrational motions play a key role in the PTR, and therefore, the assignment of the vibronic bands is important to get further insight into the dynamics of the PTR. The observed spectrum shows the broad features, and the vibrational progression consists of at least two low-frequency intermolecular modes with the spacing of 98 and 120 cm^{-1} [18]. In C_{2h}-symmetry, the dimer has six intermolecular vibrational modes and three of them are optically allowed. As will be described in Sections II-1-2 and II-2, these three vibrational modes observed in the spectrum of tautomeric dimer are 72, 80, and 107 cm^{-1} and they are at 55, 67, and 109 cm^{-1} for the similar model base pair, $(1\text{-AC})_2$ [18]. In the spectrum of $(7\text{-AI})_2$ in Figure 2b, however, only two vibrational modes were detected. The spectrum reported in the latter study has also only two low-frequency modes [41]. Recently, Kato and Shirota examined the low-frequency Raman-active intermolecular vibrational modes of 7-azaindole in CCl_4 by a femtosecond Raman-induced Kerr effect spectroscopy [42]. They observed the hydrogen-bonding vibrational bands of $(7\text{-AI})_2$ in CCl_4 at 89 cm^{-1} and 105 cm^{-1}. Their calculated frequencies of three Raman-active modes below150 cm^{-1} are 91 cm^{-1} for a stagger (out-of-plane rocking) (γ_{bg}) mode, 96 cm^{-1} for a wheeling (in-plane asymmetric rocking) (δ_{ag}) mode, and 109 cm^{-1} for an intermolecular symmetric stretching (ν_{ag}) mode. They assigned the observed 89 and 105 cm^{-1} bands to the overlap of the γ_{bg} and δ_{ag} modes, and to the νag mode, respectively. These arguments suggest that the δ_{ag} and γ_{bg} modes of the excited-state $(7\text{-AI})_2$ might be also overlapped in the gas-phase spectrum. But, in the tautomeric dimer as described in II-1-2, the lower band is split to two bands [18]. The higher frequency (120 cm^{-1}) of the ν_{ag} mode in the excited state implies that the hydrogen bonds become stronger in the excited state.

The other interesting feature of the spectrum in Figure 2b is the strong vibrational progressions start at the 740 cm^{-1} band, which exhibit the very similar spectral pattern to that of the origin [18]. Most of these bands are ascribed to the fundamentals, overtones, and combination bands of the aforementioned intermolecular vibrations. Close inspection of this spectrum shows a weak intermolecular vibrational progression starts at 950 cm^{-1}. Recently, Brause, et al. examined the absorption and fluorescence spectra of 7-AI monomer and determined the change in structure upon electronic excitation by the Franck-Condon analysis for the progression counter of the emission spectrum [43]. Based on the detailed analyses, they assigned the 715 cm^{-1} band in Figure 2a to a pyridine-ring puckering mode. This vibration mode includes the pyridine ring breathing motion and is

the only mode associating with a large displacement of the N atom among those with the vibrational modes of less than 1000 cm^{-1}. Since the dimer spectrum exhibits the broad features, there is no clear evidence to assign the band at 740 cm^{-1} in Figure 2b to that originated from the 715 cm^{-1} mode in monomer; a precise calculation is required to assign the vibration frequencies of the excited-state dimer. The electronic spectra of water clusters with 7-AI, which were found to form strong doubly hydrogen bonds similarly to $(7\text{-AI})_2$, have a vibronic band at 740 cm^{-1} from the band origin [16,35]. Thus, the 740 cm^{-1} band observed in the spectrum of $(7\text{-AI})_2$ can be assigned to the pyridine-ring breathing mode. In Section II-4-1, the role of these intra and intermolecular vibrations in the PTR will be discussed in more detail.

(II-1-2) Spectroscopy of 7-AI tautomeric dimer

In order to figure out the potential energy surface and to understand the dynamics of the ESPTR of the model base pair, the spectroscopic information on the product, in the present case, the tautomeric dimer, is also indispensable. As described in the Section III-1, the normal dimer is thermodynamically stable than the tautomeric dimer in the ground state. Thus, it is difficult to prepare the tautomeric dimer with any conventional methods. The fluorescence experiments of $(7\text{-AI})_2$ indicate that the normal dimer emits the visible fluorescence from the tautomer with high efficiency, which suggests that the excitation of the normal dimer may efficiently yield the tautomeric dimer in the ground state as a reaction product, through the ESPTR followed by the emission processes. This prediction was successfully proved to be true in solution by Tokumura, et al. [11,12,29], and later by Chou, et al. [30]. Using a two-step excitation method, they succeeded in trapping the tautomeric dimer and observed the spectrum of the S_1-S_0 transition, which starts at about 420 nm and peaks at 360 nm [12]. The lifetime determined was 19 μs at 298 K and 180 μs in the low-temperature matrix (172 K). These experimental findings strongly suggested that the tautomeric dimer would be trapped even in the gas phase, if the excess energy in the tautomeric dimer deposited in the emission process could be removed by a suitable relaxation process, such as collisions with the carrier gases. In order to produce a jet-cooled dimer in the tautomeric form, the normal dimer in supersonic expansion was excited by a KrF excimer laser (248 nm) at about 1 mm downstream from a nozzle exit. The excited-state dimer undergoes the PTR, forming the tautomeric dimer, which relaxes to the ground state mainly through the emission process. Since the density of the carrier gas at the point where the laser beam cross with the molecular beam is still high and the multiple collisions remove the excess internal energy, the tautomeric dimer is stabilized and effectively cooled down to a ultra-cold condition.

Figure 3 shows the fluorescence excitation spectrum of 7-AI tautomeric dimer thus produced, recorded by monitoring the visible emission monitored through a glass filter [18]. The origin of the

transition to the first excited state was observed at 23071 cm^{-1}. Starting from this transition, a long progression with a vibrational spacing of 107 cm^{-1} was observed. In addition to this mode, two other vibrational modes of 72 and 80 cm^{-1} were observed. Similarly to the spectrum for normal $(7\text{-AI})_2$, the highest frequency mode was assigned to the intermolecular symmetric stretching (ν_{ag}) mode, while those of two low frequency modes were assigned to the in plane (δ_{ag}) and out of plane rocking (γ_{bg}) modes. In contrast to the rocking modes, the ν_{ag} vibration exhibits the long progression up to v = 9 with a single node peaking at v = 4. These results indicate that the transition is from the zero vibrational level in the ground state and is consistent with the features of the Frank-Condon envelops observed in the dispersed fluorescence spectra, which are not shown [18]. In the dispersed fluorescence spectra, two intermolecular vibrational modes having 123 cm^{-1} and 93 cm^{-1}spacings were observed; the higher mode have a long progression [18]. These vibrations were assigned to the symmetric stretching and bending modes, respectively. The results clearly show that the ground-state potential along the symmetric stretching coordinate is shorter in the length and deeper in the well than that in the excited state.

II-2. Spectroscopy of 1-AC monomer and its dimer

The $(7\text{-AI})_2$ dimer is the best target to investigate the PTR process, but the spectroscopic information on the excited state of this dimer is rather limited because of its diffuse spectral features as described in Section II-1. The similar molecule having a hydrogen-donating N-H and a hydrogen-accepting N atom is 1-azacarbazole (1-AC) (see Figure 1b), which has a benzene ring at the pyrrole side of 7-AI, and could be a alternative candidate to gain further insight into the potential energy surface and the dynamics of PTR in the excited state. In 1-AC, the addition of benzene ring expands the π conjugate system, and as a result, the reaction may become much slower, because the basicity of pyridine ring and the acidity of pyrrole ring in the excited-state are expected to be weaker than those of $(7\text{-AI})_2$. El-Byoumi, et al. first reported the dual fluorescence of $(1\text{-AC})_2$ in solution as was observed for $(7\text{-AI})_2$, and determined the energy barrier height for the ESPTR as 2.95 kcal/mol by the temperature dependence of the visible fluorescence intensity [7]. Since then, several research groups examined the spectroscopic properties and reactivity in solution. The $S_1 - S_0$ transition was observed at 367 nm in solution [8,9]. These solution studies demonstrated the slower ESPTR process than that of $(7\text{-AI})_2$, which promises to gain rich information on the relation between the structure and dynamics of the reaction. Up to now, the gas-phase study has been limited only to our earlier works [17-19]. Because the results on these spectroscopic studies help us to get deeper understanding on the dynamical aspect of PTR, we reanalyze the experimental data and summarize the spectroscopic results on 1-AC and its dimers in this section.

The electronic spectra of 1-AC and its dimers were examined using the fluorescence excitation and mass-selected MPI methods. The fluorescence excitation spectrum of 1-AC monomer exhibits a vibrationally-resolved spectrum having the 0-0 transition at 30338 cm^{-1}. The spectrum was well corresponded to the excited-state vibrations of jet-cooled carbazole [44].

The fluorescence excitation spectrum for the dimer, which is shown in Figure 4, shows the vibrational progression starting at 28556 cm^{-1}, and it was assigned to the $S_1 - S_0$ transition [17]. As expected, the dual emission was found in the UV and visible regions; the latter fluorescence peaks at 20500 cm^{-1}. However, the yield of the visible emission is much lower than that of $(7\text{-AI})_2$. Using a picosecond time-resolved fluorescence technique as described in the Section II-3, the visible emission was ascribed to that from the tautomeric dimer. Figure 4 shows the fluorescence excitation spectrum of $(1\text{-AC})_2$ obtained by monitoring the visible fluorescence. The spectrum shows the clear origin at 28556 cm^{-1} and the well resolved vibrational bands with a long progression of a 109 cm^{-1} mode. Again the spectrum exhibits the large red shift by 1782 cm^{-1} from that of monomer suggesting the formation of strong double hydrogen bonds. The observed progressions were assigned to the combinations and overtones of three intermolecular vibration modes as in those of $(7\text{-AI})_2$; the fundamental frequencies were 55, 67, and 109 cm^{-1}, respectively. From the comparison with $(7\text{-AI})_2$, the highest-frequency vibration was assigned to the ν_{ag} mode, while the other two vibrations were ascribed to the γ_{bg} (55 cm^{-1})and δ_{ag} (67 cm^{-1})modes, respectively. The other interesting feature is that, for the overtone and combination bands of the ν_{ag} vibration, the spectral intensities in the excitation spectrum by monitoring the visible fluorescence are more enhance than those by monitoring the UV fluorescence [18]. The ratios of these spectral intensities, which give a qualitative estimate for the rate of the ESPTR, are consistent with the reaction rates determined by the time-resolved experiments which are discussed in details in Section II-3. We also tried to trap a tautomeric dimer of $(1\text{-AC})_2$ in molecular beam as was done for $(7\text{-AI})_2$, but, we could not detect the visible emission from the tautomer; we observed the strong emissions from the fragments such as C_2 molecule, suggesting that some other reactions proceed with a relative high yield [45]. The results are consistent with that of the dispersed fluorescence spectrum, which shows much lower visible emission yields of $(1\text{-AC})_2$ as low as less than 5 % of the UV emission [18].

It is instructive to note that the heterodimer (7-AI)(1-AC) formation also takes place, the studies of which provide new information on the PTR process [17]. The spectral properties and reactivity of the heterodimer were investigated in the jet cooled condition, and they were very similar to those found for $(1\text{-AC})_2$. The fluorescence excitation spectrum recorded by monitoring the visible emission showed a large spectral shift by 1825 cm^{-1}, which was slightly larger than that of $(1\text{-AC})_2$. As in those of the homodimer $(7\text{-AI})_2$ and $(1\text{-AI})_2$, the spectrum of the heterodimer in the lower energy region consists

of the progressions of the fundamental, overtones and combination bands of the 61, 90, and 114 cm^{-1} modes.

II-3. Time resolved studies and mechanism of PTR in model base pairs.

The time-resolved study of the PTR of $(7\text{-AI})_2$ on picosecond time scale was first started by Hetherington et al., who found that the proton transfer takes place on a time scale shorter than 5 ps [10]. They proposed two possible pathways, a direct tautomerization from nonequilibrated dimers and an indirect path through thermally equilibrated dimers. In order to improve the time resolution, Share et al. studied the ESPTR of $(7\text{-AI})_2$ in solution with the fluorescence gating and transient absorption techniques using a femtosecond laser (0.3 ps) [13]. They determined the time constant of 1.4 ps for the protonated and 4.0 ps for the deuterated species. Based on a transient absorption experiment, they also proposed another channel, through which the ground-state tautomer was formed within the time scale of the laser pulse width.

As described in Introduction, in 1995, Douhal, et al. reported the time-resolved study of the ESPTR of $(7\text{-AI})_2$ in molecular beam using a mass spectrometry coupled with a femtosecond laser technique [20]. They observed a double-exponential decay and it excitation energy dependence; their time constants are 650 fs and 3.3 ps by the excitation at about zero excess energy, and 200 fs and 1.6 ps by the excitation at 1.5 kcal above the zero vibrational level. Based on these results, they concluded that the ESPTR process proceeds through the two step path: the first proton transfer takes place on a time scale of a several hundred femtoseconds, and then the second proton transfer proceed more slowly with the picosecond time scale. Folmer, et al. also studied the PTR of jet-cooled $(7\text{-AI})_2$ with a Coulomb explosion technique and deduced that an intermediate product was formed in 700 fs and decayed within a picosecond time scale. Their experimental results support the above study of Douhal, et al. [46]. Douhal, et al. further reexamined the PTR in solution using a fluorescence gating technique and proposed the non-concerted mechanism on the basis of the observation of two-component rise of tautomer fluorescence [21]. On the other hand, Takeuchi and Tahara reexamined extensively the PTR of $(7\text{-AI})_2$ in solution using a femtosecond fluorescence up-conversion technique in a series of papers [22,47]. They also observed the two-component rise of tautomer fluorescence (0.2 and 1.1 ps), but ascribed the fast component to the decay of the higher excited state. It is because this fast component is not affected at all by deuterium substitution, which implies that the decay has no correlation with the proton translocation. Thus, their conclusion for the mechanism is the concerted pathway, in which two protons in the dimer transfer simultaneously. After these studies, several research groups argued on the mechanism of PTR for more than 6 years. Details of the debates were reviewed by Sakota and Sekiya [24]. Here, we briefly summarize these studies and the kinetic mechanism of the PTR reaction of $(7\text{-AI})_2$ both in solution and in the gas phase.

In solution, Takeuchi and Tahara thoroughly investigated the fluorescence of $(7\text{-AI})_2$ by using the up-conversion method and showed that the decay time constant of the normal dimer excited at near

the gas-phase origin agrees with the rise time of tautomer [47]. On the other hand, Kwon and Zewail also examined the equilibrium constant (K_{eq}) and the PTR rate of $(7\text{-AI})_2$ in several solvents including acetonitrile (ACN); the time constants are varied from 1.1 to 2.1 ps depending on the solvent [48]. From the observed small polarity dependence of the reaction rate, they concludes again the stepwise mechanism.

In the gas phase, Sakota, et al. reexamined the vibrationally-resolved decay rates of $(7\text{-AI})_2$ using two-color MPI technique with picosecond laser pulses having a cross correlation time of 2.7 ps [49]. They reported the decay time profiles at the origin and at the fundamental of the ν_{ag} mode, and determined the time constants as 1.9 ± 0.9 ps and 860 ± 300 fs, respectively. Based on these data, they claimed that the decay profiles of $(7\text{-AI})_2$ were fitted well with the single-exponential functions, which indicate no stable intermediate state in the ESPTR. However, their results in the gas phase seem to be not conclusive yet because of the limitation in time resolution used in their experiments as was pointed out by Zewail [48]. In related to these analysis, it has to be recalled that the excited-state $(7\text{-AI})_2$ has the low frequency vibrational levels, in which the PTR takes place with the different reaction rates as shown in the earlier studies [18]. The lifetime measurement in the gas phase with a femtosecond laser technique may give only an averaged time constants of several vibronic levels. It should be emphasized that, in the time-resolve experiments, we need to consider the energy resolution as well as the time resolution. Unfortunately, for $(7\text{-AI})_2$, the reaction rate is so fast to obtain enough high time resolution for the excitation energy dependence. To determine the reaction mechanism irrefutably, the most straightforward method is to detect both the reactant and product, and scrutinize the consistency of their temporal behaviors as was performed in the gas phase [19] and in solution [47]. From this point of view, the MPI techniques frequently used may not be an appropriate method to examine the mechanism of the PTR of $(7\text{-AI})_2$, because both the reactant and product have the same mass number, and because the ionization potentials of the intermediate and products participated in the reaction are unknown [50]. Moreover, if the laser intensity used is enough high, the observed ion signals may include the product ions formed in the reaction processes through the higher-energy states and possibly through the ionic states, in addition to those from the first exited state. As a result, the simple mass-detection techniques may be not suitable to track the reaction dynamics of moderately complex molecule such as $(7\text{-AI})_2$. Thus, the mechanism of the gas-phase PTR process of $(7\text{-AI})_2$ derived from the time-dependent experiments might not be conclusive yet. However, it is worth to notice that the reaction intermediates predicted theoretically in the step-wise mechanism have the zwitterionic and/or charge transfer characters [25,26] and they are expected to be much stabilized in solution than in the gas phase. Therefore, much more large solvent effects than reported by Kohn and Zewail may be predicted from the computation studies. If we consider the observed PTR rate in the gas phase as described above (1.9 ps at the zero-vibrational level [49]) and these arguments, their discussion on

polarity dependence of the PTR rate to support the stepwise mechanism may have no basis [51]. Although there may still remain the other point to be addressed, the mechanistic results indicating the agreement of the dimer-decay and tautomer-rise time constants reported by Tahara's group [47] strongly suggest that the tautomeric dimer is formed directly from the normal dimer without the mediation of any reaction intermediate in solution. These solution results may also implicitly support that the PTR of $(7\text{-AI})_2$ also proceeds with the single-step manner in the gas phase.

To circumvent the difficulty in elucidating the mechanism of the ESPTR of model base pair, we chose the other dimer $(1\text{-AC})_2$ in our earlier study [19]. This dimer exhibits the very similar PTR process that the $(7\text{-AI})_2$ dimer does, but less reactive so that the fluorescence from both the normal and tautomeric dimers are detected. Figure 5 shows the decay of the UV fluorescence of the reactant at the v = 1 level of the ν_{ag} mode (trace a) and the rise and decay of the visible fluorescence of the product (trace b) observed with a time-correlated single-photon counting method of enough high energy and time-resolutions. As it is clearly seen, the decay of normal dimer is a single exponential, and its time constant (130 ps) agrees with that of the rise time of tautomer fluorescence within an experimental errors. This finding conclusively supports the originally proposed concerted mechanism, in which no intermediate is mediated in the reaction. We also determined the PTR rates from several intermolecular vibrational levels with a precision enough to discuss the vibrational mode specific reactivity, which is directly related to the dynamics of the PTR as described in Section II-4-1.

II-4. Potential energy surface and dynamics of proton transfer reaction (PTR).

In order to understand the dynamics of the PTR process in hydrogen-bonded systems, information on the potential energy surface is crucially important. However, in general, the experimental investigation to probe the potential energy surface is difficult because most of the reactions take place in solution. The model base pairs such as $(7\text{-AI})_2$ and $(1\text{-AC})_2$ are considered to be the best examples among various PTR systems, because the reactions of these dimers are observed in molecular beam as well as in solution. These systems provide us a wealth of spectroscopic information on the potential energy surface and the dynamical aspect of PTR. Here, we summarize the spectroscopic characteristic in potential energy surfaces though some of them were reported in the earlier studies. As described in II-1-1, the visible-fluorescence excitation spectra of $(7\text{-AI})_2$ and $(1\text{-AC})_2$ in the energy regions of $< 500\ cm^{-1}$ above the origin consist of the vibrational bands ascribed to three intermolecular vibrational modes such as the ν_{ag} , δ_{ag} , and γ_{bg} modes [18]. The fluorescence spectra of both the normal and tautomeric dimers of $(7\text{-AI})_2$ exhibit the long progressions of the ν_{ag} mode, which is the reaction coordinate of PTR: the progression of the normal dimer is observed at least up to v=4 as seen in Figure 2b. Especially, in the spectrum of $(7\text{-AI})_2$ tautomer, the fluorescence and dispersed fluorescence spectra

exhibit the well resolved vibrational progressions of the ν_{ag} mode up to at least v' = 9 as seen in Figure 3. The calculations on the excited-state potential surfaces of $(7\text{-AI})_2$ by Ando, et al. [25] indicate that the energy difference between the reactant and product is ca. 0.42 eV and that the above spectral range covers one-third of the potential well of the product side. As described in Sec. II-1-1 and II-1-2, the frequencies of the ν_{ag} mode of the normal dimer are 105 (in solution [42]) in the ground and 120 cm^{-1} [18] in excited states, while they are 123 and 107 cm^{-1} [18] for the tautomeric dimer. These results clearly indicate that the potential well depth along the symmetric stretching coordinate in the excited-state normal dimer is deeper than that in the ground state, while those are reversed in the tautomeric dimer. In addition to the energetic aspects of the potential energy surfaces, the vibrational mode specific features of the PTR were observed for the first time in $(7\text{-AI})_2$ and $(1\text{-AC})_2$ among various PTR systems as mentioned in the next subsection.

(II-4-1) Vibrational mode dependence of PTR

The PTR in polyatomic molecules takes place on the multidimensional potential energy surface [3,52-56]. In order to understand the proton transfer dynamics, it is important to find the spectroscopic indications of the reaction in the spectroscopic data. The spectroscopy of the jet-cooled PTR system allows us to explore the reactivity from each single vibronic level, and thus provides us information on vibrational mode specific reactivity, which may give a direct insight into the dynamics which is coupled to the degrees of vibrational freedom. Since the supersonic molecular beam technique was introduced in the field of molecular spectroscopy in early 1980's [57], various PTR systems found in solution were reexamined in molecular beam to observe the vibrational mode specific reactivity. However, almost all of the systems were found to be nonreactive in a jet-cooled condition, except for a few systems including the present model base pairs [17,18]. These systems may enable us to explore the dynamical mechanism which promotes the PTR through the intra- and intermolecular vibrational excitations.

As Figure 2b clearly shows, the spectral band widths of $(7\text{-AI})_2$ change rapidly with increasing the vibrational quantum number: the bandwidth of the ν_{ag} mode increases rapidly as 5, 10, and 30 cm^{-1} for n = 0, 1, and 2, respectively. On the other hand, the fundamental level of the rocking band at 90 cm^{-1} exhibits the narrower bandwidth of 3 cm^{-1}. The width increases to 7 cm^{-1} for the combination band with one quantum of the ν_{ag} vibration [18]. Because the observed spectrum is the action spectrum of the PTR process, the increase in the bandwidth corresponds to the lifetime shortening of the vibronic state due to the enhanced reactivity. As described in Section II-3, the time resolved experiment of the single vibronic levels for $(7\text{-AI})_2$ is difficult and limited only to a few lowest vibration bands; the lifetimes of the origin and the fundamental of the ν_{ag} vibration were estimated as 1.9 ± 0.9 and 0.86

±0.3 ps, respectively [49]. Although the values have fairly large experimental errors due to the limited time resolution, they are consistent with the values estimated from the bandwidths above.

Until now, the vibrational mode dependence of the PTR for these dimers has been examined only for the intermolecular vibrations. In addition, the participation of an intramolecular vibration is also expected in the proton translocation through the N—H···N hydrogen bonds of dimer [18]. As analyzed in Section II-1-1, the vibronic bands of 7-AI monomer observed below 1000 cm^{-1} above the electronic origin were assigned to the ring deformation vibrations. Among them, some of the in-plane vibrations are possibly coupled with the ν_{ag} vibration, and take part in the reaction. From this viewpoint, the spectrum of $(7\text{-AI})_2$ in Figure 2b should be reexamined carefully. The bandwidth of the vibronic band above 350 cm^{-1} of the origin is more than 50 cm^{-1}, which indicates the much faster reaction at the higher overtone level of the ν_{ag} vibration. This result is consistent with the energy barrier height estimated for the ESPTR of $(7\text{-AI})_2$ in solution as 490 cm^{-1} [6]. On the other hand, the bandwidths of the groups of vibronic bands staring at the 740 cm^{-1} band, which is assign to the intramolecular pyridine-ring breathing mode, are not so broad, compared with the intermolecular modes of above 350 cm^{-1} of the origin, even though the vibrational energy of this band exceeds the energy barrier height. The bandwidth of the 740 cm^{-1} and the 740 +120 (=860) cm^{-1} bands are about 8 and 21 cm^{-1}; the latter band is the combination band with the ν_{ag} mode. They are compatible with those of the band origin and of the +120 cm^{-1} band (5 and 10 cm^{-1}). Thus, the relatively narrow spectral width of the 740 cm^{-1} band and those associated with this band seem to indicate that the rate of the PTR depends not directly on the excess vibrational energy, but it is strongly vibrational mode specific. Taking into account the intensities of the latter bands, the 740 cm^{-1} vibration plays a role in the PTR, but not so prominent as the ν_{ag} vibration. The other interesting point is that the weak progressions of the intermolecular vibrations start at 974 cm^{-1} above the origin. As described in Section II-1-1, the 974 cm^{-1} band may correspond to the 940 cm^{-1} band of 7-AI monomer, which was assigned to the 18b mode and observed as a strong peak in Figure 2a. The weak intensity of this vibration in the action spectrum suggests a minor role of this mode in PTR. Therefore, from these analyses as well as the absence of the other intramolecular vibrational bands in the action spectrum, the intramolecular vibrational modes with the frequencies of less than 1000 cm^{-1} are less important than the ν_{ag} mode.

As analyzed already, the PTR in $(1\text{-AC})_2$ proceeds much more slowly than in $(7\text{-AI})_2$ and therefore the rates from the single vibronic levels could be examined in more details with both the spectroscopic and time-resolved measurements [19]. The fluorescence lifetimes of the vibrational levels near the origin were measured in molecular beam using the single photon counting technique coupled with a picosecond laser. In Figure 4, together with the fluorescence excitation spectrum by monitoring the visible emission, the reaction rates at various vibrational levels are plotted. The open circles are for the

PTR rates at the zero vibrational level and at the fundamental and overtone levels of the ν_{ag} vibration (109 cm^{-1}). The reaction rate increases almost exponentially by the excitation of this mode as 3 x 10^9 s^{-1}, 7.7 and 15.5 x 10^9 s^{-1}, respectively. On the other hand, the rates at the γ_{bg} (55 cm^{-1}) and δ_{ag} (67 cm^{-1}) vibrational excitations, shown by triangle and square, are slightly suppressed as 2.7 and 2.8 x 10^9 s^{-1}, respectively. It can be noticed that, once the ν_{ag} mode participates in the combination levels, the rate increases substantially; 6.7 x 10^9 s^{-1}at 55 + 109 and 7.7 x 10^9 s^{-1}at 67 + 109 cm^{-1}. The ratio to that of the corresponding fundamental mode is nearly about 2. These findings are consistent with the reaction rates estimated from the intensity ratios of the fluorescence excitation spectra measured by monitoring the UV and visible emissions [18]. The latter measurements also exhibit a further reduction of the PTR rates from the overtone levels of the above two rocking modes indicating a substantially strong suppression effect of these vibrational motions. Thus, both $(7\text{-AI})_2$ and $(1\text{-AC})_2$, the strong enhancement of the PTR rate by the excitation of the ν_{ag} vibration, and the suppression by the excitations of the two rocking modes are consistently observed. Similar enhancement and suppression by the mode-specific vibronic excitations were also reported later for the deuterated $(7\text{-AI})_2$ [39].

In our previous paper [18], we discussed the dynamical effect of the vibration modes qualitatively using a schematic 2-dimensional (2D) potential energy surface by taking the N—H and the intermonomer distances as the reaction coordinates. In the zero order approximation, the dynamical effect of the ν_{ag} motion in the PTR is the shortening (lengthening) of the N—N distance. However, the above findings clearly indicate that the PTR of model base pairs is strongly coupled with the other intra- and inter-molecular modes, having the multidimensional nature. Thus, it might be premature to discuss the role of the ν_{ag} vibration without further information on the intramolecular vibration such as the N—H stretching (ν_{NH}) mode, which may also play an important role in the dynamical mechanism of PTR. In relation to this issue, Guallar, et al. carried out semiclassical molecular dynamics calculations to simulate the dynamics of the PTR of $(7\text{-AI})_2$ using the reduced dimensional potential energy surface constructed with the calculated energies by the CIS method [58]. Unfortunately, their potential energy surface used in simulation has the minimum at a zwitterionic intermediate, which implies that their potential energy surface is incompatible with the experimental findings. Their simulations carried out were on the hypothetical surface. Thus, their results cannot be used as reference in the present arguments. In order to get further insight into the dynamical role of the ν_{ag} vibration in the ESPTR of the model base pairs, the theoretical studies of the reaction dynamics and of the analysis of the spectroscopic data are required on more appropriate multidimensional potential energy surfaces, which should include the intramolecular N—H stretching and the intermolecular modes, and the dynamical couplings among them.

(II-4-2) Tunneling effect on PTR

The possible contribution of the tunneling to the PTR processes has been frequently discussed from

the beginning [1]. In the current model base pairs, the temperature-dependent fluorescence experiments strongly suggested an important role of the simultaneous proton tunnelings, where the energy barrier heights in solution were estimated as 1.4 kcal/mol (490 cm^{-1}) for $(7\text{-AI})_2$ [6] and 2.95 kcal/mol (1030 cm^{-1}) for $(1\text{-AC})_2$ [7]. The reaction through the proton tunneling was also found in the gas phase PTR of $(7\text{-AI})_2$ and $(1\text{-AC})_2$ [17,18]. As described in Sections II-1-1 and II-2, both dimers emit the visible fluorescence from the tautomeric dimers even with the excitation at the zero vibrational level of the S_1 state. And also, the nearly-exponential increase in the reaction rates by the excitation of the overtones of the ν_{ag} vibration is a clear indication of the existence of the energy barrier and of the contribution from the proton tunneling through the reaction barrier. For $(7\text{-AI})_2$, we attempted to examine the deuteration effect on the PTR rates in the visible-fluorescence excitation spectra of singly and doubly deuterated dimers [18]. However, we failed to assign the 0 - 0 band of the doubly deuterated dimers, $(7\text{-AI})_2$-*dd*, because it is heavily superimposed over the +98 cm^{-1} band of the nondeuterated dimer, $(7\text{-AI})_2$-*hh*. Sakota, et al. reexamined the deuteration effect and revised the assignments [41]. Following the spectroscopic study on isotopically mixed benzene dimers [59], they assigned three origin bands of the deuterated dimers of $(7\text{-AI})_2$-*h*d*, $(7\text{-AI})_2$-*hd**, and $(7\text{-AI})_2$-*dd* to the bands observed at +41, +62 and +96 cm^{-1} above that of non-deuterated dimer $(7\text{-AI})_2$-*hh* (32256 cm^{-1}), respectively. They also estimated the PTR rates of four isomers, k^{hh}, k^{h*d}, k^{hd*}, and k^{dd}, as 5 x 10^{11}, (9.8 ± 0.6) x 10^9, (6.9 ± 1.1) x 10^9, and (7.0 ± 1.0) x 10^8 s^{-1}, respectively, from the intensity ratios of the UV and visible emission in the dispersed fluorescence spectra.

The similar deuterium substitution experiments were also carried out for $(1\text{-AC})_2$ in molecular beam [18]. Figures 6a and 6b show the fluorescence excitation spectra of the deuterated dimers by monitoring the visible and UV emissions, together with the corresponding result on non-deuterated dimer in Figure 6c. These results are reanalyzed in this paper. The origins of three deuterated isomers, $(1\text{-AC})_2$-*h*d*, $(1\text{-AC})_2$-*hd**, and $(1\text{-AC})_2$-*dd*, were observed at 22, 38, and 57 cm^{-1} above the origin of non-deuterated dimer $(1\text{-AC})_2$-*hh* (28556 cm^{-1}). As in the spectrum of $(7\text{-AI})_2$, the origin band of $(1\text{-AC})_2$-*dd* is heavily superimposed over the γ_{bg} band at 57 cm^{-1} of $(1\text{-AC})_2$-*hh*. Fortunately, their intensity can be quantitatively determined by taking into account the intensity ratio of the 57 and 68 cm^{-1} bands of $(1\text{-AC})_2$-*hh*. Because the reaction yields of these dimers are low (< 0.05) as described in Section II-2, the spectral intensities in the UV-monitored spectrum are a good measure of the relative concentrations of four isotopomers in molecular beam. Using these spectral intensities and those of these isotopomers in the visible-monitored spectrum, the ratio of the relative PTR rates of $(1\text{-AC})_2$-*hh*, $(1\text{-AC})_2$-*h*d*, $(1\text{-AC})_2$-*hd**, and $(1\text{-AC})_2$-*dd* were estimated as 1.0 : 0.03 : 0.17 : 0. The PTR rate of $(1\text{-AC})_2$ is strongly reduced by the deuterium substitutions as was found for $(7\text{-AI})_2$ and the reaction in $(1\text{-AC})_2$-*dd* suppressed within an experimental error. Thus, we conclude that both $(7\text{-AI})_2$ and $(1\text{-AI})_2$ exhibit the prominent kinetic isotope effect (KIE) ($k^{hh}/k^{dd} > 10^2$).

The ratio k^{h*d}/k^{hd*} of the PTR rate of heterodimers for $(7\text{-AI})_2$ was determined to be 1.4 by Sakota,

et al. [39]. Because the excited-state heterodimers, *h*d* and *hd**, have the similar reaction rates, they concluded the predominance of the concerted reaction path. Zewail and coworker also estimated k^{hh}, k^{h*d}, k^{hd*}, and k^{dd} by proton inventory experiment as 9 x 10^{11}, (5.4 ± 0.6) x 10^{11}, (2.0 ± 0.2) x 10^{11}, and (1.1 ± 0.3) x 10^{8} $s^{-1}$for $(7\text{-AI})_2$, respectively, in solution [48]. Based on the deviation from the predicted geometric mean ($k^{h*d} \neq k^{hd*} \neq (k^{hh}k^{dd})^{1/2}$, k^{h*d}/k^{hd*}=2.7), they derived the opposite mechanism of the stepwise path. On the other hand, the above results for $(1\text{-AC})_2$ gives a much smaller value, k^{h*d}/k^{hd*}=0.2. As emphasized in the preceding subsection, this dimer was confirmed to proceed through the single-step reaction [19]. Thus, these experimental results and the arguments suggest that it is difficult to relate straightforwardly the KIE value with the reaction mechanism. It should be noted that the potential energy surface of the excited state is not symmetric for two molecules (See the computational results [26]). An important point is that the above experimental findings clearly indicate the prominent role of the tunneling effect in the PTR of both $(7\text{-AI})_2$ and $(1\text{-AC})_2$. And besides, the KIE values could not follow the rule of a simple geometrical mean, because the ESPTR rates of these dimers are determined by the tunneling process on the multi-dimensional surface, and therefore by the coupling with the other inter- and intra-molecular vibrational motions

(II-4-3) Recent theoretical studies on potential energy surface

The potential energy surface of the ESPTR of $(7\text{-AI})_2$ has been the subject of intensive theoretical studies, however, most of the studies are concerned with the potential surfaces including the intermediate states [26]. The recent advances in the theoretical and computational methods allowed to calculate the reliable potential energy surface for describing the single-step reaction path, which is compatible with the experimental findings. Ando, et al. [25] investigated the reaction mechanism by constructing a full dimensional empirical valence bond potential energy function (PEF) based on the potential energies evaluated by ab initio molecular orbital methods, and carried out quantum dynamics calculations with the PEF. Their potential energy surfaces of the PTR determined at the multi-reference perturbation level of theory favors a concerted PTR mechanism. They also examined the possibility of the stepwise mechanism where a CT state is involved as an intermediate. The energy crossing seams between the localized excited state and the CT one lie at about 5 kcal/mol higher than the transition state energy. They concluded that the energy crossing seams to the CT state is unlikely to be reached by the 0–0 excitation; only with a certain amount of excess energy, the reaction path to a stepwise path through the CT state becomes open. Taketsugu, et al. [26] also examined the excited-state double proton transfer in the $(7\text{-AI})_2$ using the complete active space second-order perturbation theory (CASPT2) method and the long-range corrected time-dependent density functional theory (LC-TDDFT) method. They examined the reaction routes for the double proton transfer in the excited state in details; They located a route having a single transition state (TS1) between the normal (N*) and tautomer (T*) dimers; the barrier height being 1.5 kcal/mol from N* to ST1 and 8.5 kcal/mol from T*

to TS1. In addition, on the excited state potential energy surface, they found two equivalent zwitterionic intermediates (Z), which lie lower by 4.9 kcal/mol than the excited normal dimer (N*). Furthermore, the transition state structure (TS2) from the zwitterionic intermediate state (Z) to the tautomer excited state (T*) is found; the barrier heights are 10.9 kcal/mol from Z to TS2, which involves the back electron and proton transfers, and 13.0 kcal/mol from T* to TS2. Though the transition state (TS3) between the zwitterionic (Z) and the normal excited dimer (N*) could not be located, the barrier height might be as high as that of TS2. The reaction through the zwitterionic states is the two-step mechanism. Based on their calculations, Taketsugu, et al. concluded that the ESPTR proceeds with the concerted mechanism at the low excitation energy. They also showed that the concerted ESPTR proceeds asynchronously in C_s symmetry rather than synchronously in C_{2h} symmetry.

As described in Section II-4-1, experimentally the prominent vibrational mode specific PTR was found; the mode specificity is the spectroscopic manifestations of the reaction dynamics. Especially, the tunneling rates in these dimers were found to be promoted by the ν_{ag} vibration. Although the vibration-assisted tunneling were studied theoretically for model system [53] and the PTR in the ground state [58], no rigorous calculations were reported for the ESPTR of the model base pairs. In this regard, Ando, et al. [25] performed the reduced two-dimensional quantum dynamics calculations on the reaction surface Hamiltonian for the PTR coordinates. They evaluated the time constants of the reaction to be on the order of picoseconds, which is consistent with experiments. However, as they pointed out, the computed kinetic isotope effect was found to deviate from the experimental data, because of a lack of the explicit treatment of the intermolecular vibrational motion in their calculations for the quantum effect. In order to understand the dynamics of the ESPTR of model base pair including the intermolecular vibrational motion, in particular, the symmetric-stretching vibration assisted tunneling, it seems to require more explicit quantum dynamics calculations.

III. PTR in the electronically ground state

The ground-state proton-transfer is a ubiquitous and very important process in such an acid-base reaction. The ground-state proton-transfer reaction (GSPTR) process in $(7\text{-AI})_2$ corresponds to the back reaction of the aforementioned ESPTR. Contrary to the ESPTR, the number of the investigations on the GSPTR of $(7\text{-AI})_2$ is much limited. Tokumura, et al. measured the transient absorption of the tautomeric dimer [11,12]. The lifetime of the tautomeric dimer in 3-methylpentane was found to be 19 μs and the activation energy barrier height of the GSPTR was estimated as 1.4 kcal/mol (490 cm^{-1}) from the tautomeric well. Chou, et al. reexamined further the GSPTR process of $(7\text{-AI})_2$ in the other hydrocarbon solvents and found that the decay rate correlates with the viscosity; 16.8 μs in heptane to

33 μs in hexadecane [30]. They also estimated the activation energy in these solvents and found that the barrier height (6.2 – 6.8 kcal/mol; 2170 – 2380 cm^{-1}) is independent of solvents within experimental error. These results indicate that the excitation energy of the N—H vibrational mode of the tautomeric dimer exceeds the activation energy of the GSPTR. Therefore the spectroscopic signature of the reaction may appear in the vibrational spectrum of the tautomeric dimer as a competing process of the intramolecular vibrational energy redistribution. For the electronically excited states, several works reported the potential energy surface as described in Section II-4 [25, 26]. However, the PES of the 7-AI ground-state dimer has not been reported. In the following sections, first, we describe the results of the theoretical calculations for the PTR of $(7\text{-AI})_2$ in the ground state to facilitate the assignment of the observed IR spectra [60]. And then, the IR spectroscopic investigations on the ground-state of the 7-AI normal and tautomeric dimers are reviewed.

III-1. Potential energy surface of the 7-AI dimer in the electronic ground-state

The potential energy surface (PES) of $(7\text{-AI})_2$ for the double proton transfer reaction from the normal dimer to the tautomeric dimer is helpful to understand reaction dynamics. Figures 7 and 8 are our DFT results obtained with the Gaussian 09 program package [61]. Figure 7 shows the energy characteristics of the two isomers and the transition state between them on the ground state; two functionals were used in the calculations. The calculated energy difference between two isomers is close to the experimentally estimated value (5800 cm^{-1}), while the activation energy barrier by a new functional (M06-2X) from the tautomer to the transition state is substantially lower than that of the experimental estimation (about 2300 cm^{-1}) [30]. The calculations give the vibrational frequencies of the symmetric and anti-symmetric N—H stretching modes of the normal $(7\text{-AI})_2$ by B3LYP as 3084 and 3120cm^{-1}, respectively, while those of the tautomeric dimer are 2532 and 2623 cm^{-1} scaled by 0.961, respectively. The calculated frequencies of the ν_{ag} mode for the normal and tautomeric $(7\text{-AI})_2$ in the ground state by B3LYP are 105 and 128 cm^{-1}, which agree with the experimental values described in Section II-1-2. The calculations also predict that the dimerization energy of 7-AI is 4286 cm^{-1} by B3LYP, while it is 4760 cm^{-1} by M06-2X functional.

In constructing the 2D PES, all the variables are optimized except for four distance variables, $R(N_1\text{-}N_2)$, $R(N_1'\text{-}N_2')$, $R(N_1\text{-}H)$, and $R(N_1'\text{-}H')$ (see Figure 8a) under the planarity constrain for the coordinates. Under these constrains, we could not locate the transition state for the stepwise mechanism on the ground state surface. The 2D PES for the concerted mechanism was constructed, with the B3LYP/6-31+G(d,p) level by assuming $R(N_1\text{-}N_2) = R(N_1'\text{-}N_2')$ and $R(N_1\text{-}H) = R(N_1'\text{-}H')$. The variables of the

PES in Figure 8 are $R_{N\text{-}N} = R(N_1\text{-}N_2)$ and $M = R(N_1\text{-}H) - R(N_2\text{'-}H)$ [25]. In PES, the filled circle is at the normal dimer configuration and the filled square is at the tautomeric dimer. The PES shows the coupling of the N—H distance M and the intermolecular distance $R_{N\text{-}N}$ in the reaction coordinate. The elongations of the N—H distance (proton transfer) must accompany the shortening of the intermolecular distance. From the experimental point of view, the necessity of such a coupling between the N—H and the intermolecular motion was emphasized by Fuke, et al. long time ago in the previous report [18].

III-2. IR spectroscopy of the 7-AI monomer and normal dimer

The IR spectrum of the 7-AI monomer in the gas phase was first reported by Cané et al. [62]. They measured the IR spectrum of the 7-AI vapor at 110 °C in the region from 100 to 4000 cm^{-1} and found that the N—H stretching (ν_{NH}) band appears at 3517.5 cm^{-1}. Later, the IR spectra of the N—H/C—H stretching region of the jet-cooled 7-AI normal monomer and dimer were observed by Yokoyama, et al. with an IR-UV double resonance spectroscopy [38]. As shown in Figure 9, the ν_{NH} band of the monomer appears at 3521 cm^{-1} with a sharp band profile. On the contrary, that of the normal dimer exhibits a very complicated band pattern centered at 3100 cm^{-1}. There is no band appearing at higher than 3200 cm^{-1}. It means that both of the N—H groups in the dimer are hydrogen-bonded to the pyridino N atom of the counterpart of the dimer, and that the symmetric dimer configuration is reconfirmed by this observation. The band profile of the jet-cooled 7-AI normal dimer shown in Figure 8 is very similar to that observed in solution [63]. This fact indicates that the solvation effect on the N—H stretching motion of the 7-AI dimer is small and that the complicated profile of the ν_{NH} band should originate from the strong coupling among the N—H modes, between the N—H and intermolecular modes, and possibly between the N—H and C—H modes in the dimer.

In order to clarify the vibrational interaction of $(7\text{-AI})_2$ in the ground state, Dreyer, et al. investigated the vibrational dynamics of the ν_{NH} band of $(7\text{-AI})_2$ in solution using a femtosecond infrared pump–probe technique [63]. They observed an extreme shortening of the vibrational population time of the N—H/N—D stretching mode upon dimer formation. The ~100 fs population decay of the N—H stretching excitations of the dimer was interpreted by highly efficient relaxation via resonant over- and combination tones of strongly coupled fingerprint modes. They also observed a coherent excitation of the low-frequency hydrogen bond stretching mode (110 cm^{-1}) induced by resonant excitation of the N—H stretching vibrations. In order to understand the complex feature of the ν_{NH} band further, Dreyer analyzed the anharmonic interactions among the ν_{NH} and the nearby levels based on the theoretical calculations [64]. He found that the combination levels involving the N—H bending character strongly interact with the ν_{NH} level through the anharmonic resonances. In the normal dimer, the N—H bending

frequency is close to those of the finger print modes such as the C—C stretching modes of the indole ring; the N—H bending character is distributed into many modes in the normal mode basis. Upon dimerization, the v = 1 level of the ν_{NH} mode is red-shifted by 400 cm^{-1} as described previously and is shifted into the energy range of 3100 cm^{-1} where the combination and overtones of the fingerprint modes are located. As a result, the band profile of the ν_{NH} mode becomes very complicated because of the Fermi resonances between the N—H v = 1 state and over and combination tones. He reproduced the complicated pattern of the ν_{NH} band of the normal dimer in solution similar to that in the gas phase shown in Figure 7 by introducing an empirical homogeneous line width of 30 cm^{-1} to bring the simulated spectrum into best agreement with the spectral broadening of the subbands in the observed spectrum.

It is worth to notice that the energy difference between the normal and tautomeric dimers in the ground electronic state is as large as about 5800 cm^{-1} estimated from the frequencies of the 0 – 0 transitions of the normal and tautomeric dimers, and the calculated energy difference of the excited-state potential wells of these dimers (0.42 eV) [25]. This value is consistent with our calculation as shown in Figure 7 and is much higher than the IR excitation energy of the v=1 level of the ν_{NH} mode. Therefore, the fast population decay of N—H stretching excitations corresponds to the intra and intermolecular vibrational relaxation processes and is not directly related to the GSPTR from the normal dimer. However, it is a good reference system when we discuss the IR spectrum of the tautomeric dimer as described below.

III-3. IR spectroscopy of the 7-AI tautomeric dimer

We successfully observed the infrared spectrum of the jet-cooled 7-AI tautomeric dimer and their deuterated dimers using the IR-VIS double-resonance technique [28,29]. Figure 10 is the IR spectrum in the region from 2400 to 3200 cm^{-1}. As described in Section III-2, in the normal dimer, the v = 1 level of the ν_{NH} mode is in the energy range of 3100 cm^{-1} where combination and overtones of several fingerprint modes are located, and as a result, the band profile of the ν_{NH} vibration becomes very complicated because of the Fermi resonance. On the other hand, for the tautomeric dimer, the calculations predicts that the red-shift of the ν_{NH} mode by the dimerization is about 800 cm^{-1}; the calculated ν_{NH} frequencies of the monomer and dimer are 3440 – 3450 cm^{-1} and 2623 cm^{-1}, respectively, at the B3LYP level. Because the redshift of the tautomeric dimer is much larger than that of the normal dimer, the energy match between the N—H v = 1 state and the over and combination tones is expected to be strongly reduced. In accord with this prediction, the observed band profile of the v = 1 level of the ν_{NH} mode is much simpler as seen in Figure 10. The sharp vibrational bands at 3080 and 3120 cm^{-1} were assigned to the C—H stretching bands of the indole ring. Similarly to the normal dimer, the

symmetric doubly hydrogen-bonded structure of the tautomeric dimer was confirmed, because a free N—H stretching band was not observed above 3200 cm^{-1}. A strong and broad band at 2676 cm^{-1} was assigned to the anti-symmetric N—H stretching mode of the tautomeric dimer by comparing with the calculated frequency of this mode (2623 cm^{-1}at the B3LYP level) as described in Section III-1. The broad spectrum is well reproduced by a sum of three Gaussian shaped bands; one broad and intense peak and two rather sharp bands. Two relatively sharp bands at 2534 and 2578 cm^{-1} with the FWHM of 34 cm^{-1} may correspond to the combination and/or overtones of some fingerprint modes. The profile of the 2676 cm^{-1} band is homogeneous with the FWHM of 245 cm^{-1}. This band profile may suggest the line broadening due to the lifetime shortening; the bandwidth gives a lower limit of the lifetime of this level as about 20 fs. As described previously, the activation energy of the back reaction of the tautomeric dimer was determined as about 2300 cm^{-1}. This value indicates that the ν_{NH} level is located above the energy barrier height. Thus the extremely broad feature of the 2676 cm^{-1} band may suggest a direct coupling of the N—H stretching level with a continuous level on the PTR surface. Although we did not detect the product in our experiment, a fast PTR may proceed through this level. The excitation energy of the v = 1 of the ν_{NH} level scaled from the bottom of the normal dimer is 8791 cm^{-1} (2676 + 5800 cm^{-1}), while the calculated binding energy between two 7-AI monomer is 4286 cm^{-1} as described in Section III-1. Thus these numbers imply that some of the products of the back PTR may dissociate into the 7-AI monomers.

Up to now, the N—H/N—D stretching modes discussed are the IR active ones corresponding to the anti-symmetric stretching vibrations in C_{2h} symmetry. This mode is not parallel to the direction of the reaction coordinate of the concerted path. The symmetric N—H/N—D stretching modes, which are the Raman active, may provide us more insight into the dynamics of the PTR of model base pair.

III-4. Deuteration effects on the IR spectra of the normal and the tautomeric dimers

In order to get further insight into the relation between the ν_{NH} vibration and the PTR process, we also examined the deuteration effect on the ν_{NH} band of both the normal and the tautomeric dimers. As described in Section III-2, the 7-AI normal dimer can be considered as a reference system that does not exhibit the PTR, and thus, the deuteration effect on the N—H/N—D band profile of the normal dimer is examined first. Figure 11 shows the N—H/N—D stretching band of the deuterated 7-AI normal dimer. The spectrum of the undeuterated dimer is also displayed for comparison. There are three isotopic species, the NH-NH (*hh*), NH-ND (*hd*), and ND-ND (*dd*) dimers, concerning the deuteration of the H atom in the N—H groups. The profile of the N—D band around 2280 cm^{-1} is not so complicated than those of the ν_{NH} bands around 3000 cm^{-1}, where the transition intensity is distributed among several excitations through the anharmonic interaction. Figure 11 clearly indicates that the N—H and/or N—D stretching band profile does not affected by the single deuteration: the change from the *hh* to the *hd* or from the *hd* to the *dd* dimers is relatively small. This fact indicates that

the anharmonic interaction of the N—H or N—D excited level is localized within the monomer unit in the dimer. The degrees of the broadening of the N—H and/or N—D stretching band for the *hd* and *dd* dimers are similar to the ν_{NH} band for the *hh* dimer.

As for the tautomeric dimer, the N—H/N—D stretching band profiles exhibit a different dependence on the deuteration. Figures 10a and 10b show the IR spectra in the N—H/N—D stretching region of the isotopomers of the tautomeric dimer. On the contrary to the normal dimer, the ν_{NH} band of the *hd* dimer exhibits the different profile than that of the *hh* dimer: a overlapped band centered at about 2550 cm^{-1} and a relatively broad band (FWHM; 117 cm^{-1}) at 2674 cm^{-1}. The latter band appears at the same spectral position to that of the 2676 cm^{-1} of the *hh* tautomeric dimer and may be assigned to the ν_{NH} band. Because the ν_{NH} bands of the *hh* and the *hd* tautomeric dimers are located above the activation energy barrier (about 2300 cm^{-1}) of the PTR process, the reduction of the bandwidth of the ν_{NH} band of the *hd* dimer by half due to the deuterium substitution is considered to be the kinetic isotope effect of the 2676 cm^{-1}band.

In the *hh* dimer, there are no fundamental bands expected in the region from 1800 to 2300 cm^{-1}. The bands below 2100 cm^{-1} in Figure 10a can be assigned as the combination bands. The *hd* and the *dd* tautomeric dimers also exhibit several bands in the same region. These bands are also assigned to the combination bands as in the case of the *hh* dimer. The bands in the region from 2050 to 2300 cm^{-1} for the *hd* and the *dd* tautomeric dimers in Figures 10b and 10c are assigned as the ν_{ND} bands. The profiles of the ν_{ND} bands of these dimers exhibit a relatively simple pattern similar to those of the ν_{ND} bands of the deuterated normal dimers shown in Figure 11, however, the bandwidths of the former are much wider than those of the normal dimer. As described in Section III-1, the activation energy barrier of the PTR determined is about 2300 cm^{-1}, which is close to the excitation energy of the ν_{ND} mode. Therefore, the broad features of the ν_{ND} bands for the *hd* and the *dd* tautomeric dimers, similar to that of the N—H band around 2600 cm^{-1} for the *hh* dimer, may indicate the opening of the fast PTR process.

IV. Summary and Outlook

In this review, we presented the experimental and theoretical studies on the PTR of model base pairs, $(7\text{-AI})_2$ and $(1\text{-AC})_2$, both in the ground and excited states. In order to fully discuss the potential energy surface and the dynamics of the PTR of these systems, we described the spectroscopic results on the monomers and dimers of 7-AI and 1-AC in molecular beam. The spectroscopic properties of the jet-cooled $(7\text{-AI})_2$ tautomeric dimer were also discussed. We also outlined the current status of the mechanistic studies on the ESPTR of these dimers. As for $(7\text{-AI})_2$, the single-step mechanism was confirmed in solution by the straightforward kinetic approach which elucidated the time coincidence of the temporal behaviors of the reactant and product fluorescence. The same approach is difficult for the PTR of jet-cooled $(7\text{-AI})_2$ because of the limited fluorescence-detection sensitivity. Thus, several

attempts were made to examine the mechanism using the MPI techniques, which could not apparently resolve the controversies because of the deficiencies inherent to the MPI techniques as discussed in Section II-3. To avoid the experimental difficulties, one of the authors carried out the time-resolved fluorescence experiments of jet-cooled $(1\text{-AC})_2$ in place of $(7\text{-AI})_2$ and confirmed the single-step path for the ESPTR. The results for $(1\text{-AC})_2$ strongly suggest that the ESPTR of jet-cooled dimer also proceeds with the single-step path. The recent theoretical calculations for $(7\text{-AI})_2$ also support the single-step mechanism.

The spectroscopic investigations of the ESPTR of the jet-cooled dimers gave us a wealth of information on the vibrational mode specific reactivity and the kinetic isotope effect exhibiting the predominance of the tunneling process in the reaction. These experimental findings allowed us to map out the excited-state potential energy surface and the reaction dynamics to proceed on it. We also presented the recent results on the PTR of the tautomeric $(7\text{-AI})_2$ in the ground state, in which we found the extremely fast reaction from the v=1 level of the ν_{NH} mode.

From the experimental points of view, these dimers have been extensively studied both in solution and in gas phase. However, there still remain several points to be addressed for a better understanding of the underlying proton transfer dynamics. In particular, for the jet-cooled $(7\text{-AI})_2$, the time-resolved fluorescence experiments of doubly deuterated dimer, whose fluorescence lifetime is an order of ns, may allow us to examine the mechanism with much better energy and time resolutions. The precise analysis of the vibrational mode specific KIE may enable us to get insight into a multidimensional feature of the tunneling process in the PTR of model base pairs. As for the GSPTR of $(7\text{-AI})_2$, we examined the reaction from the optically allowed antisymmetric N—H stretching vibrational level. The similar experiment with a Raman detection is particularly challenging because one can prove the reactivity of the symmetric N—H stretching vibrational level. Since the $(7\text{-AI})_2$ tautomeric dimer exhibits the long progression of the symmetric stretching vibration, the laser spectroscopy with a stimulated emission pumping method may make it possible to explore the potential energy surface near the activation barrier.

Recent advances in theoretical calculations can yield the reliable potential energy surface, which support the experimentally derived reaction mechanism; in the present case, the single step path. There are more rich of the unexplored issues in the theoretical studies for the proton transfer reactions. For instances, the vibrational mode specific reactivity and the vibrational-motion assisted multidimensional tunneling have not been examined for real molecular systems such as for $(7\text{-AI})_2$, and will be one of the most important targets in the works combined with the quantum chemical and reaction dynamic theories in near future. These studies reveal the characteristic of the potential energy surfaces for the proton transfer reactions in more detail and strive toward a better understanding of the

dynamics of the PTR of model base pairs. These theoretical efforts will lead to more general idea and concepts for the PTR in widely spread molecular systems, for example, on the role of the surrounding heavy atoms in translocating the proton and on the role of the multi-dimensional nature of the reaction surface in the tunneling reaction.

Acknowledgements

We thank Prof. Suehiro Iwata for critical reading of this manuscript. We also thank Dr. Kohei Ando for helpful communications on recent theoretical calculations of $(7\text{-AI})_2$ and for discussion of some of his unpublished results on this dimer. This work is partially supported by the Grant-in-Aid for Scientific Research (Grants # 24350009) from the Ministry of Education, Culture, Sports, Science, and Technology (MEXT) of Japan.

References

[1] P.-O. Löwdin, Adv. Quantum Chem. 2 (1965) 213.
[2] A. Jefrey, W. Saenger, *Hydrogen Bonding in Biological Structures*; Springer-Verlag: Berlin, 1991.
[3] V. A. Benderskii, D. E. Makarov, C. A. Wight, Adv. Chem. Phys. 88 (1994) 1.
[4] C. A.Taylor, M. A. El-Bayoumi, M. Kasha, Proc. Natl. Acad. Sci. U.S.A. 63 (1969) 253.
[5] K. C. Ingham, M. Abu-Elgheit, M. A. El-Bayoumi, J. Am. Chem. Soc. 93 (1971) 5023.
[6] K. C. ngham, M. A. El-Bayoumi, J. Am. Chem. Soc. 96 (1974) 1674.
[7] C. Chang, N. Shabestary, M. A. El-Bayoumi, Chem. Phys. Lett. 74 (1980) 107.
[8] J. Sepiol, U. P. Wild, Chem. Phys. Lett. 93 (1982) 204.
[9] J. Waluk, A. Grabowska, B. Pakula, J. Sepiol, J. Phys. Chem. 88 (1984) 1160.
[10] W. M. Hetherington, III, R. H. Micheels, K. B. Eisenthal, Chem. Phys. Lett. 66 (1979) 230.
[11] K. Tokumura, Y. Watanabe, M. Itoh, Chem. Phys. Lett. 111 (1984) 379.
[12] K. Tokumura, Y. M. Watanabe, M. Itoh, J. Phys. Chem. 90 (1986) 2362.
[13] P. Share, M. Pereira, M. Sarisky, S. Repinec, R. M. Hochstrasser, J. Lumin. *48/49*, (1991) 204.
[14] Y. Chen, R. L. Rich, F. Gai, J. W. Petrich, J. Phys. Chem. 97 (1993) 1770.
[15] K. Fuke, Y. Yoshiuchi, K. Kaya, Y Achiba, K. Sato, and K. Kimura, Chem. Phys. Lett. 108 (1984) 179.

[16] K. Fuke, H. Yoshiuchi, K. Kaya, J. Phys. Chem. 88 (1984) 5840.
[17] K. Fuke, T. Yabe, N. Chiba, T. Kohida, K. Kaya, J. Phys. Chem. 90 (1986) 2309.
[18] K. Fuke, K. Kaya, J. Phys. Chem. 93 (1989) 614.
[19] K. Fuke, K. Tsukamoto, F. Misaizu, K. Kaya, J. Chem. Phys. 95 (1991) 4074.
[20] A. Douhal, S. K. Kim, A. H. Zewail, Nature London 378 (1995) 260.
[21] M. Chachisvilis,T. Fiebig, A. Douhal, A. H. Zewail, J. Phys. Chem. A 102 (1998) 669.
[22] S. Takeuchi, T. Tahara, Chem. Phys. Lett. 277 (1997) 340 .
[23] J. Catalan, J. C. del Valle, M. Kasha, Proc. Natl. Acad. Sci. U.S.A. 96 (1999) 8338.
[24] H. Sekiya, Sakota, Bull. Chem. Soc. Jpn. 79 (2006) 373.
[25] K. Ando, S. Hayashi, S. Kato, Phys. Chem. Chem. Phys. 13 (2011) 11118.
[26] X.-f. Yu, S. Yamazaki, T. Taketsugu, J. Chem. Theory Comput. 7 (2011) 1006 and the references therein.
[27] H. Ishikawa, H. Yabuguchi, Y. Yamada, A. Fujihara, K. Fuk**e,** J. Phys. Chem. A 114 (2010) 3199.
[28] H. Ishikawa, T. Nakano, T. Takashima, H. Yabuguchi, K. Fuke, Chem. Phys. 419 (2013) 101.
[29] K. Tokumura, Y. Watanabe, M. Udagawa, M. Itoh, J. Am. Chem. Soc. 109 (1987) 1346.
[30] P. T. Chou, W. S. Yu, Y. C. Chen, C. Y. Wei, and S. S. Martinez, J. Am. Chem. Soc. 120 (1998) 12927.
[31] K. H. Hassan, J. M. Hollas, J. Mol. Spectrosc. 138 (1989) 398.
[32] A. Nakajima, M. Hirano, R. Hasumi, K. Kaya, H. Watanabe, C. C. Carter, J. M. Williamson, T. A. Miller, J. Phys. Chem. A 101 (1997) 392.
[33] M. Schmitt, C. Ratzer, K. Kleinermanns, W. Leomeerts, Mol. Phys. 102 (2004) 1605.
[34] C. Kang, J. T. Yi, D. W. Pratt, Chem. Phys. Lett. 423 (2006) 7.
[35] S. K. Kim, E. R. Bernstein, J. Phys. Chem. 94 (1990) 3531.
[36] K. Sakota and H. Sekiya, J. Phys. Chem. A 113 (2009) 2663.
[37] J. W. Young, Z. D. Pozun, K. D. Jordan, D. W. Pratt, J. Phys. Chem. B 117 (2013) 15695.
[38] H. Yokoyama, H. Watanabe, T. Omi, S. Ishiuchi, M. Fujii, J. Phys. Chem. A 105 (2001) 9366.
[39] K. Sakota, H. Sekiya, J. Phys. Chem. A 109 (2005) 2722.
[40] Y. N. Svartsov1, M. Schmitt, J. Chem. Phys. 128 (2008) 214310.
[41] K. Sakota, A. Hara and H. Sekiya, Phys. Chem. Chem. Phys. 6 (2004) 32.
[42] H. Shirota, T. Fukuda, T. Kato, J. Phys. Chem. B 117 (2013) 16196.
[43] R. Brause, M. Schmitt, D. Krugler, K. Kleinermanns, Mol. Phys. 102 (2004) 1615.
[44] A. R. Auty, A. C. Jones, D. Phillips, Chem. Phys. 103 (1986) 163.
[45] K. Fuke, unpublished results.
[46] D.E. Folmer, L. Poth, E.S. Wisniewski, A.W. Castleman Jr., Chem. Phys. Lett. 287

(1998) 1.
[47] S. Takeuchi, T. Tahara, Proc. Natl. Acad. Sci. USA 104 (2007) 5285.
[48] O. H. Kwon, A. H. Zewail, Proc. Natl. Acad. Sci. USA 104 (2007) 8703.
[49] K. Sakota, C. Okabe, N. Nishi, H. Sekiya, J. Phys. Chem. A 109 (2005) 5246.
[50] R. Lopez-Martens, P. Long, D. Solgadi, B. Soep, J. Syage, Ph. Millie, Chem. Phys. Lett. 273 (1997) 219.
[51] They claimed the stepwise mechanism based on the small polarity dependence of the decay time constants, especially on the result in ACN. However, the latter value is almost the same as that in the gas phase within experimental error (Ref. 49).
[52] V. K. Babamov, R. A. Marcus, J. Chem. Phys. 74 (1981) 1790.
[53] T. Carrington, Jr., W. H. Miller, J. Chem. Phys. 84 (1986) 4364
[54] N. Sato, S. Iwata, J. Chem. Phys. 89 (1988) 2832.
[55] S. Takada, H. Nakamura, J. Chem. Phys. 102 (1995) 3977.
[56] K. Giese, M. Petkovic, H. Naundorf, and O. Kuhn, Physics Reports 430 (2006) 211.
[57] D. H. Levy, Ann. Rev. Phys. Chem. 39 (1980) 197.
[58] V. Guallar, V. S. Batista, W. H. Miller, J. Chem. Phys. 110 (1999) 9922.
[59] K. O. Bornsen, H. L. Selzle, E. W. Schlag, J. Chem. Phys. 85 (1986) 1726.
[60] N. Shida, P. F. Barbara, J. E. Almlof, J. Chern. Phys. 91 (1989) 4061.
[61] H. Ishikawa, K. Fuke, unpublished results.
[62] M.J. Frisch, et al., Gaussian 09, Revision C. 01, Gaussian, Inc., Wallingford, CT,2010.
[63] E. Cane, P. Palrnieri, R. Tarroni, A. Trombetti, J. Chem. Soc. Faraday. Trans. 90 (1994) 3213.
[64] J.R. Dwyer, J. Dreyer, E.T. J. Nibbering, T. Elsaesser, Chem. Phys. Lett. 432 (2006) 146.
[65] J.R. Dwyer, J. Chem. Phys. 127 (2007) 054309.

Figure Captions

Figure 1. (a) Schematic of potential energy curves of $(7\text{-AI})_2$ in the ground and excited states and PTR on these surfaces.
(b) Normal and tautomeric dimers of 1-AC.

Figure 2. (a) Fluorescence excitation spectrum of jet-cooled 7-AI monomer. The peak at 34639 cm^{-1} is the origin of the $S_0 - S_1$ transition. (b) Fluorescence excitation spectrum of $(7\text{-AI})_2$ by monitoring

the visible emission from the tautomer peaks at 480 nm.

Figure 3. Fluorescence excitation spectrum of jet-cooled tautomer formed through the excited-state PTR process.

Figure 4. Fluorescence excitation spectrum of jet-cooled $(1\text{-AC})_2$ by monitoring the visible emission from the tautomer peaks at 500 nm. The PTR rates from each vibronic bands are plotted: open circles are origin, fundamental, and overtone of intermolecular symmetric stretching vibrations, while the open-triangles and –squares are fundamentals and combination bands with the former vibration, respectively. These results clearly indicate that PTR of model base pairs is strongly vibrational mode specific.

Figure 5. Temporal data for the decays of the (a) UV and (b) visible emissions of $(1\text{-AC})_2$ obtained by the excitation of the 109 cm^{-1} band in Figure . The solid lines are computer fits of the data that take into account the time response of our apparatus and the (a) single exponential and (b) biexponential functions. The decay of total emission [trace (c) 1] is also shown for comparison. (cited from Ref. 18)

Figure 6. Fluorescence excitation spectra of deuteriated 1-AC dimers obtained by monitoring visible (a) and UV (b) emissions, respectively. For comparison, the spectrum of the undeuteriated dimer (c) is also presented. In Fig. 6b, the +0, +22, +38 and +57 cm^{-1} bands correspond to the origins of *hh*, *h*d*, *d*h*, and *dd* isotopomers, respectively. The intensities of three spectra are normalized to the +67 cm^{-1} bands of each traces.

Figure 7. Relative energies among the three conformations of the 7-AI dimer. The relative energy, ΔE, is measured form the normal dimer. The unit is in cm^{-1}. The values in square brackets are measured from the tautomeric dimer.

Figure 8. (a) Labels of atoms in 7-AI dimer. (b) 2D PES of the 7-AI dimer. The interval of the contour lines is 5 kcal/mol.

Figure 9. IR spectra of the jet-cooled 7-AI (a) monomer and (b) normal dimer. (Cited from Ref. 38)

Figure 10. IR spectra of the jet-cooled 7-AI tautomeric dimer and its deuterated species.

Figure 11. IR spectra of the jet-cooled 7-AI normal dimer and its deuterated species.

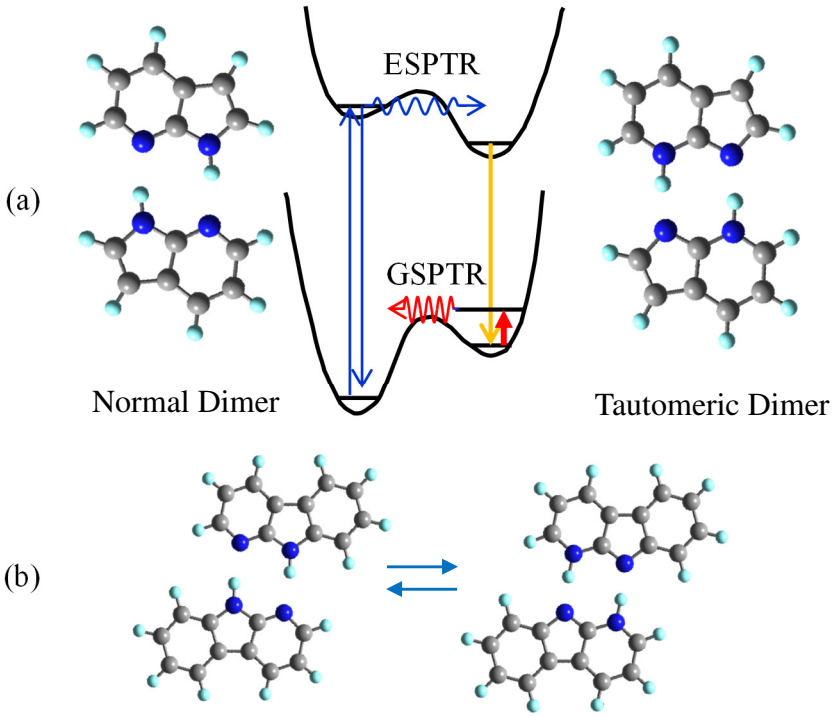

Figure 1

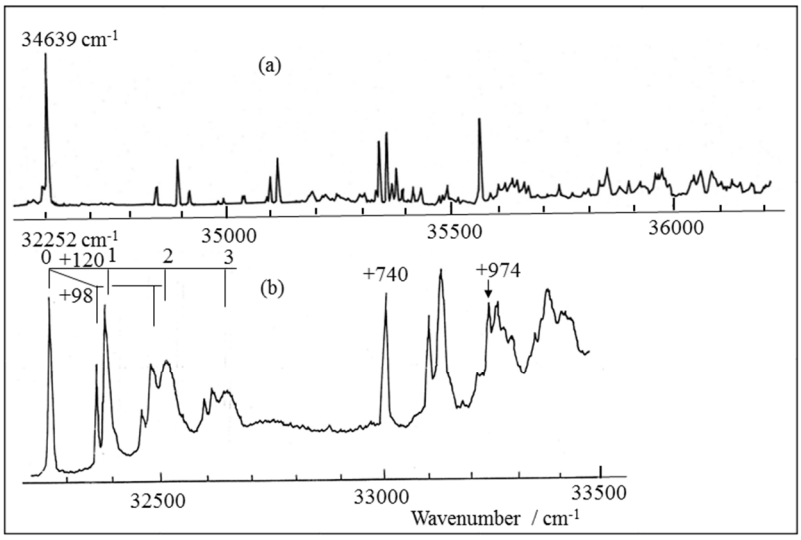
34639 cm-1
(a)
35000
35500
36000
32252 cm-1
0 +120 1 2 3
+98
(b)
+740
+974
32500
33000
33500
Wavenumber / cm-1

Figure 2

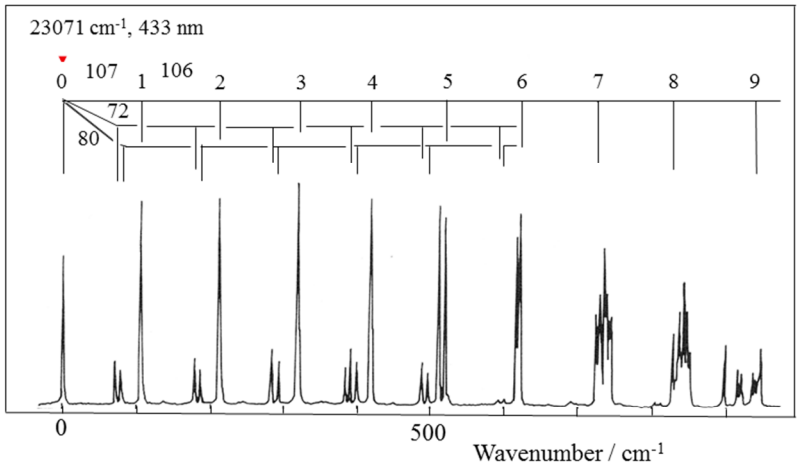
23071 cm-1, 433 nm
0
107
1
106
2
3
4
5
6
7
8
9
72
80
0
500
Wavenumber / cm-1

Figure 3

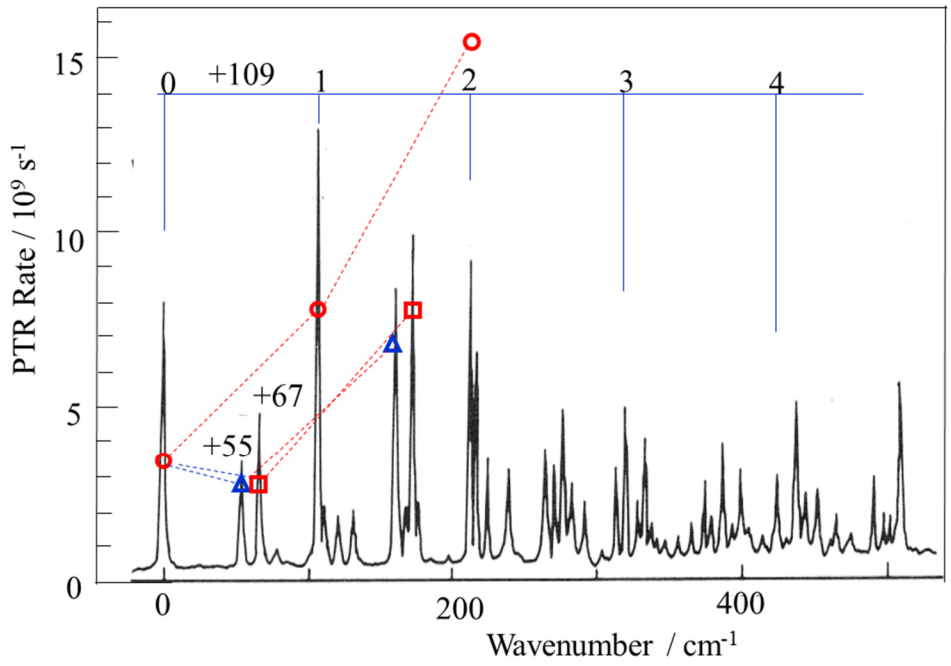
15
10
5
0
PTR Rate / 10^9 s^-1
0
+109
1
2
3
4
+67
+55
0
200
400
Wavenumber / cm^-1

Figure 4

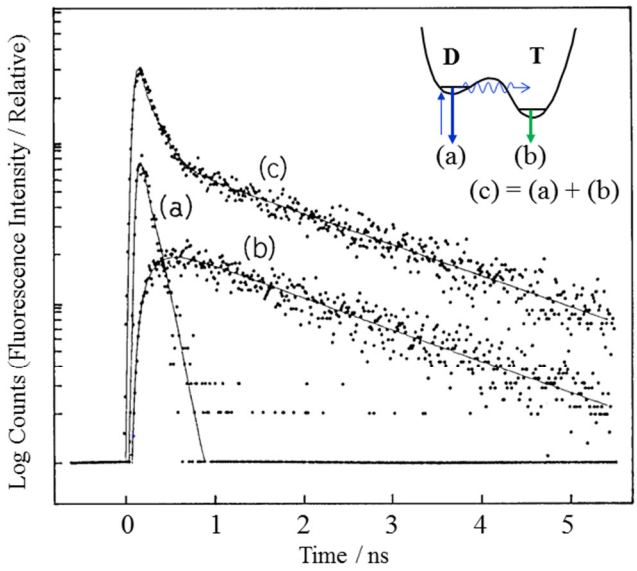
Log Counts (Fluorescence Intensity / Relative)
Time / ns
0
1
2
3
4
5
(a)
(b)
(c)
D
T
(a)
(b)
(c) = (a) + (b)

Figure 5

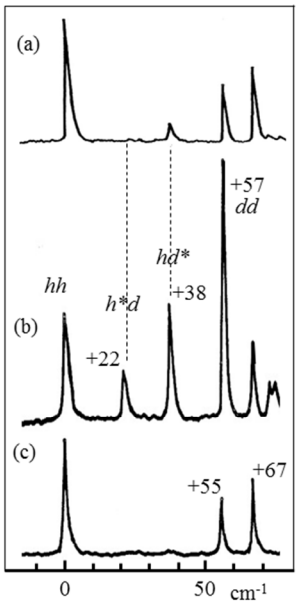

Figure 6

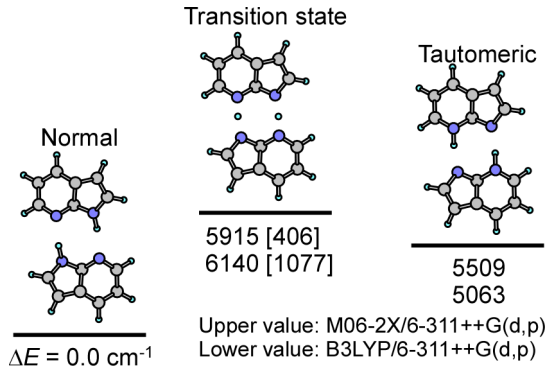
Transition state
Tautomeric
Normal
5915 [406]
6140 [1077]
5509
5063
Upper value: M06-2X/6-311++G(d,p)
Lower value: B3LYP/6-311++G(d,p)
ΔE = 0.0 cm-1

Figure 7

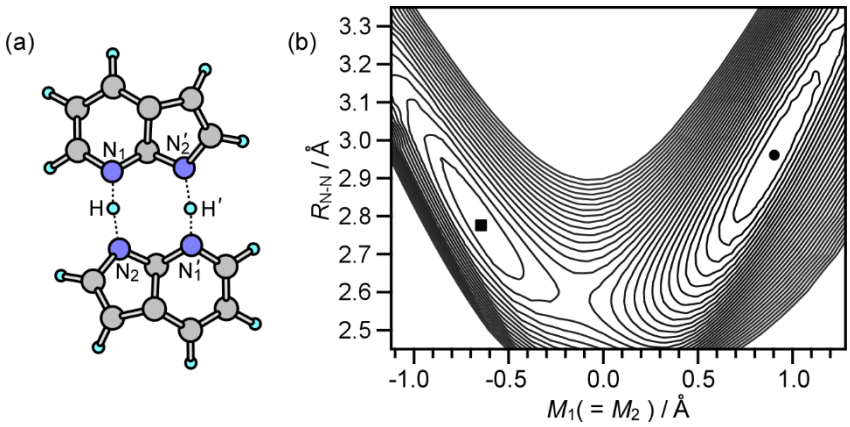

Figure 8

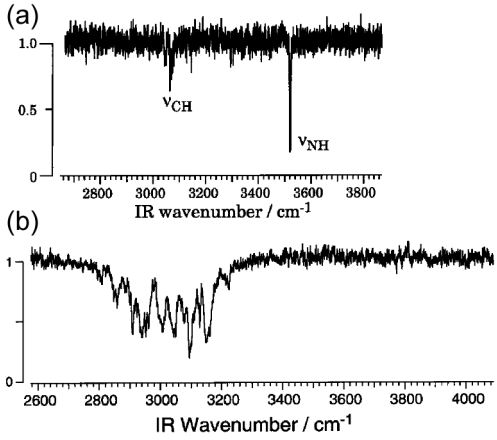
(a)
1.0
0.5
0
ν_{CH}
ν_{NH}
2800
3000
3200
3400
3600
3800
IR wavenumber / cm^{-1}
(b)
1
0
2600
2800
3000
3200
3400
3600
3800
4000
IR Wavenumber / cm^{-1}

Figure 9

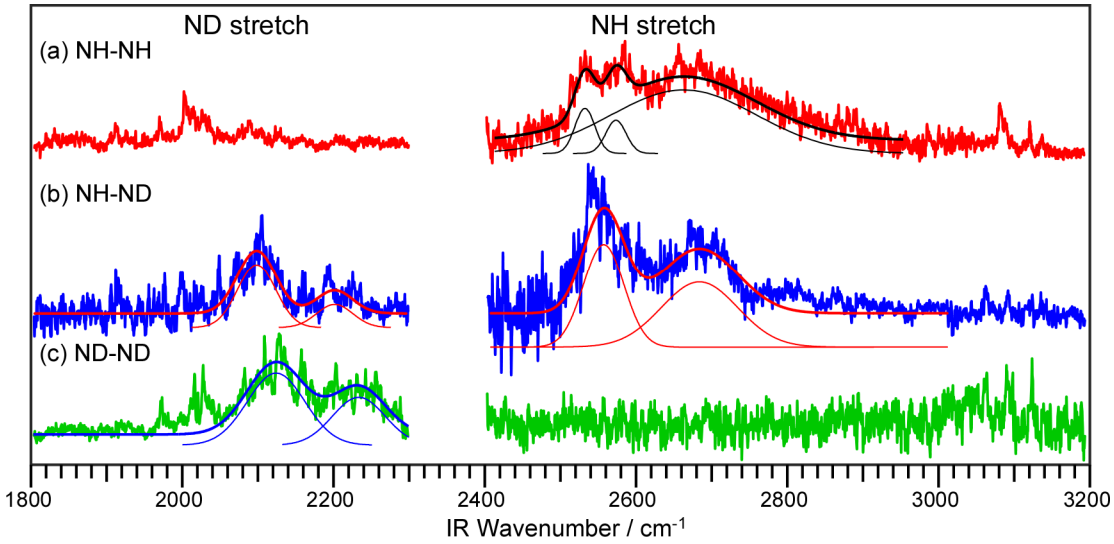
ND stretch
NH stretch
(a) NH-NH
(b) NH-ND
(c) ND-ND
1800
2000
2200
2400
2600
2800
3000
3200
IR Wavenumber / cm-1

Figure 10

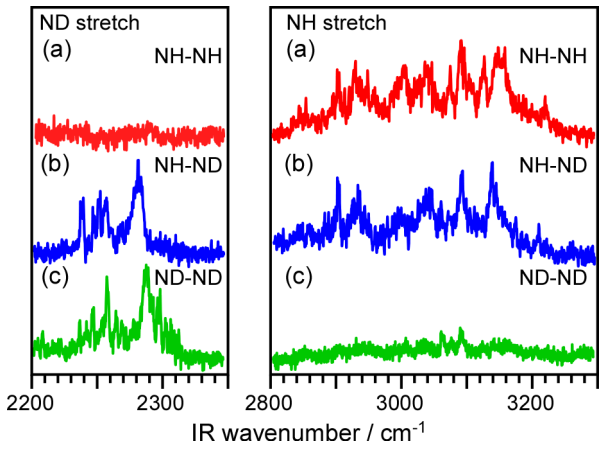
ND stretch
(a)
NH-NH
(b)
NH-ND
(c)
ND-ND
NH stretch
(a)
NH-NH
(b)
NH-ND
(c)
ND-ND
2200
2300
2800
3000
3200
IR wavenumber / cm-1

Figure 11